New Decomposition Scheme of Canal Surfaces for Planar Sections Computing

Jinyuan Jia[1], Ajay Joneja[2] and Kai Tang[3]

[1]Zhuhai College of Jilin University, csjyjia@yahoo.com.cn
[2]Hong Kong University of Science & Technology, joneja@ust.hk
[3]Hong Kong University of Science & Technology, mektang@ust.hk

ABSTRACT

Canal surfaces are applied widely in CAD and graphics. Subdivision scheme plays an important role in many geometric operations on canal surfaces. This paper develops a new quadric-based subdivision scheme that is numerically more stable, and computationally more efficient than the other quadric subdivision scheme. In addition, singularity and planar sections computing of canal surfaces are examined in this paper and some experimental results are presented.

Keywords: canal surfaces, revolute quadrics, revolute quadric-sphere, intersections

1. INTRODUCTION

A canal surface $K(t,\theta)$, generated by a parameterized spine curve $\boldsymbol{C(t)}$, in $\mathbf{R}^3$ is the envelop of spheres with radius function $R(t)$ centered at $\boldsymbol{C(t)}$. When $R(t)$ is a constant, we get pipe surfaces that are used commonly in shape reconstruction or robotic path planning. Canal surfaces are useful in representing long thin objects such as poles, 3D fonts, brass instrument or internal organs of the body in solid/surface modeling and CG/CAD. It includes natural quadrics (cylinder, cone and sphere), revolute quadrics, tori, pipes and Dupin cyclides. Therefore, many algorithms of geometric computing around canal surfaces have been developed recently [6, 7, 8, 11, 12, 13, 14, 15, 16, 17, 18, 19, 20] and [22], in which the decomposition schemes of canal surfaces play an important role. Quadrilateral or triangular subdivision is a general decomposition scheme employed for arbitrary surfaces. However, specific geometric properties of canal surfaces can be employed for more efficient decomposition schemes. We develop a new, revolute quadric-based decomposition scheme for canal surfaces, and our results demonstrate tremendous improvement in representation capability as well as computational efficiency for several intersection problems using our decomposition.

2. BACKGROUND

Three specialized decomposition schemes have been proposed canal surfaces: (*i*) circle decomposition, (*ii*) cone-sphere decomposition and (*iii*) cyclide decomposition. In circle decomposition, a canal surface is subdivided as a densely set of characteristic circles along its spine curve. It reduces various geometric computations on canal surfaces to the corresponding ones on circles. This scheme was used to solve computing of intersection curves, isophote, perspective silhouette and distance on canal surfaces in [11, 12, 13, 14] and [15]. In cone-sphere decomposition, a canal surface is subdivided as a set of spheres along spine curve. Neighboring sampling spheres are joined by a common tangential truncated cone. The entire surface is thus approximated by a series of alternating truncated cones and spherical strips. This scheme is proposed in [17], but has two drawbacks: (i) a very dense set of cone-sphere pairs is required at high precision, and (ii) when the canal surface bends with a large curvature, two neighboring truncated cones may intersect each other, breaking the spherical stripe into an open slice (instead of a band); this case is called self-intersection. In cyclide decomposition [19], a canal surface is subdivided as a group of bounded Dupin cyclide pairs by using a technique analogous to circular biarc fitting, based on Cyclographic mapping in Laguerre geometry. This is the most natural decomposition scheme for canal surfaces. However, cyclide is the fourth-degree surface and its related geometric computations have no closed form solutions mostly, e.g. intersection problems of two cyclides surprisingly need to solve 16th multi-polynomial equations. Usually, this decomposition could not effectively reduce the complexity of geometric computations of canal surfaces.

Quadrics are the lowest order curved surfaces. They have good parametric and implicit forms. Some related geometric computations are relatively easy and simple. Therefore, how to construct a piecewise quadric net of a surface becomes

important in CAGD and much research has focused on constructing a piecewise quadric spline to approximate an arbitrary surface. Powell and Sabin [21] proposed a piecewise GC^1 quadric interpolant over a triangular mesh with prescribed normal vectors, many extensions have been proposed for constructing a general Powell-Sabin interpolant. Dahmen [3] and Guo [9, 10] constructed a tangent-plane continuous piecewise triangular quadric net by using the implicit Bezier form and the split idea of Powell-Sabin for bivariate GC^1-piecewise quadric interpolation respectively. Froumentin and Chaillou [5] proposed a simple piecewise quadric interpolant by using simplex B-splines. While their approaches are purely algebraic, Bangert and Prautzsch [2] devised a geometric GC^1 piecewise quadric interpolant, by providing a geometric interpretation to certain parameters, it treats Powell-Sabin quadric interpolant as a special case. Several works have discussed how to construct a convex Powell-Sabin interpolant efficiently [1, 23, 24].

However, while suitable for general surfaces, the aforementioned schemes become inefficient or too complicated when they are directly applied to special surfaces. It is natural to explore development of specific quadric decomposition schemes for special surfaces such as canal surfaces. Cone-sphere is a common quadric decomposition scheme for canal surfaces. It is inefficient at the high precision and becomes inaccurate if the spine curve is highly curved, or the radius varies too rapidly. In this paper, we propose a revolute quadric-spherical stripes (RQ-sphere) decomposition for *regular* canal surfaces, which can avoid the above two problems of the cone-sphere scheme. The main idea is to sample a set of spheres along the spine curve appropriately and construct a common tangential revolute quadric between each pair of adjacent sampling spheres, instead of the common tangential truncated cone, to approximate the canal surface. We note that the RQ-sphere scheme is a natural extension of cone-sphere decomposition scheme with the following advantages. Compared to the cone-sphere scheme, (*i*) it can fit canal surfaces more flexibly to avoid self-intersection and yield visually smother rendering; (*ii*) it has one degree-of-freedom to allow optimal approximation of canal surfaces, and (*iii*) RQ-Sphere decomposition of the same approximation quality requires fewer RQ-sphere pairs.

The RQ-sphere decomposition scheme only works for regular canal surfaces because there is a possible self-intersection at singular points (see Fig. 1). At such points, the proposed RQ-sphere decomposition fails to approximate the canal surface. Elsewhere, we shall present an analysis of how to determine singularities, and how to decompose irregular canal surfaces; in the following, we only present some of the results that are required to check for regularity. The rest of our paper is organized as: §3 presents a sufficient and necessary condition for determining singularity of canal surfaces and present a simple way to compute the normal vector of canal surfaces; §4 proposes the RQ-sphere decomposition for a regular canal surface; §5 addresses computing planar section of canal surfaces with RQ-sphere decomposition; and §6 some examples are illustrated and §7 concludes the paper with a discussion on extensive applications of our results.

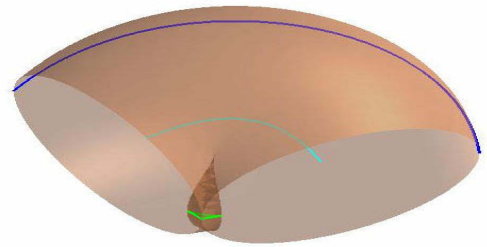

Fig. 1. Singular canal surface with self-intersection.

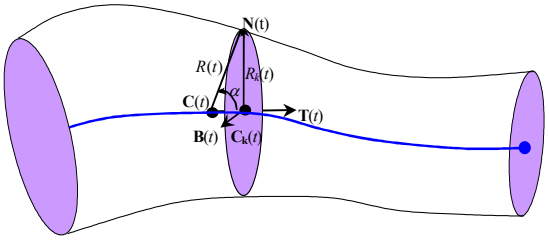

Fig. 2. Schematic of canal surface with characteristic circle.

3. ANALYSIS OF CANAL SURFACES

We assume a canal surface, with a regular spine curve $\mathbf{C}(t)$ and a rational radius function $R(t)$, is valid, namely $||\mathbf{C}'(t)|| \neq 0$, and $||\mathbf{C}'(t)||^2 - R(t)^2 > 0$. $\mathbf{C_k}(t)$ (or $\mathbf{M}(t)$ in Fig. 2) and $R_k(t)$ are the center point and the radius of its characteristic circle. Then its equation $K(t,\theta)$ can be given as the following *Frenet* form ($\mathbf{T}(t)$, $\mathbf{N}(t)$, $\mathbf{B}(t)$) of $\mathbf{C}(t)$, which determines the orientation of characteristic circle:

$$\mathbf{K}(t,\theta) = \mathbf{C_k}(t) + R_k(t)(\cos(\theta)\mathbf{N}(t) + \sin(\theta)\mathbf{B}(t)) \tag{1}$$

where $C_k(t) = C(t) - R(t)R'(t)C'(t)/\|C'(t)\|^2$ and $R_k(t) = R(t)\sqrt{\|C'(t)\|^2 - R'(t)^2}/\|C'(t)\|$

In the case where the spine curve $\mathbf{C}(t)$ is planar, $\mathbf{T}(t)$ = (x'(t), y'(t), 0), $\mathbf{B}$(t) = (0, 0, 1) and $\mathbf{N}(t) = (-y'(t), x'(t), 0)/\sqrt{x'(t)^2 + y'(t)^2}$.

Since the method presented in our approach cannot handle canal surfaces with singularities, we present here a result that helps us to identify such surfaces.

Theorem 1. Given a canal surface $\mathbf{K}(t,\theta)$ in Eq. (1) with a spine curve $\mathbf{C}(t)$ and a radius function $\mathbf{R}(t)$, it is a singular if the following equations have solution:

(i) $R_k(t) = 0$,

(ii) at some (t_0, θ_0),

$$\|\mathbf{C}'(t)\| - \frac{R'(t)^2 + R(t)R''(t)}{\|\mathbf{C}'(t)\|} + \frac{R(t)R'(t)\langle \mathbf{C}'(t), \mathbf{C}''(t)\rangle}{\|\mathbf{C}'(t)\|^3} - R_k(t)\|\mathbf{C}'(t)\|\cos(\theta)\kappa(t) = 0.$$

Proof: For brevity, we omit some details of the proof here. By definition, a surface $\boldsymbol{K}(t,\theta)$ is singular if and only if $\mathbf{K}_t(t,\theta)\times\mathbf{K}_\theta(t,\theta) = 0$, where the subscripts indicate partial derivatives with respect to the indicated parameter. We express the partial derivatives of $\boldsymbol{K}(t,\theta)$ from eqn (1) in the Frenet form. Some algebraic manipulations then lead to the proof. Without showing derivations, the partial derivatives are:

$$\mathbf{K}_t(t,\theta) = \left(\|\mathbf{C}'(t)\| - \frac{R'(t)^2 + R(t)R''(t)}{\|\mathbf{C}'(t)\|} + \frac{R(t)R'(t)\langle \mathbf{C}'(t), \mathbf{C}''(t)\rangle}{\|\mathbf{C}'(t)\|^3} - R_k(t)\|\mathbf{C}'(t)\|\kappa(t)\cos(\theta) \right)\mathbf{T}(t) \tag{2}$$
$$+ \left(R_k'(t)\cos(\theta) - R_k(t)\|\mathbf{C}'(t)\|\tau(t)\sin(\theta) - \kappa(t)R(t)R'(t)\right)\mathbf{N}(t) + \left(R_k'(t)\sin(\theta) + R_k(t)\|\mathbf{C}'(t)\|\tau(t)\cos(\theta)\right)\mathbf{B}(t)$$

$$\mathbf{K}_\theta(t,\theta) = R_k(t)\left(-\sin(\theta)\mathbf{N}(t) + \cos(\theta)\mathbf{B}(t)\right). \tag{3}$$

We note that for a general canal surface, checking for singularity must be carried out numerically since the system of equations resulting from Theorem 1 is high-degree multivariate. The analysis can be somewhat simplified for some special cases, e.g. when the spine curve is planar. Nevertheless, such computation can be considered an up-front setup cost, and our main focus in this paper is run-time efficiency of regular canal surfaces. The following sections deal with the latter issue.

4. RQ-SPHERE DECOMPOSITION OF CANAL SURFACES

We address three problems: (*i*) how to construct a simple RQ-Sphere fitting a canal surface for two given sampling spheres on the spine curve, (*ii*) how to determine the optimal local fit between a RQ-Sphere and the canal surface and (*iii*) how to globally optimize the approximation of a canal surface with a set of RQ-Sphere pairs.

4.1 Construction of Local RQ-Sphere Fitting

We construct a local coordinate system with the centers of two sampling spheres S_1 and S_2 at (0, 0, 0) and (*c*, 0, 0) respectively as shown in Fig. 3*a* , and the revolute axis of the common tangential revolute quadric of S_1 and S_2 as *x*-axis. Then

Sphere S_1: $x^2 + y^2 = r^2$ (4)

Sphere S_2: $(x-c)^2 + y^2 = R^2$ (5)

Revolute quadric RQ: $Ax^2 + y^2 + Dx + F = 0$ (6)

By substituting Eq. (4) into Eq. (6), we get a quadratic equation $(A\text{-}1)x^2 + Dx + (F+r^2) = 0$, since the RQ is tangential to S_1, its determinant must be zero:

$$\Delta_1 = D^2 - 4(A-1)(F+r^2) = 0 \tag{7}$$

Similarly by substituting Eq. (5) into Eq. (6), we get equation $(A\text{-}1)x^2 + (D+2c)x + (F + R^2 - c^2) = 0$, its determinant also should be zero, since RQ is tangential to S_2:

$$\Delta_2 = (D+2c)^2 - 4(A-1)(F+R^2-c^2) = 0. \tag{8}$$

From Eq. (7) and Eq. (8), we obtain the other two coefficients *D* and *F* as functions of *A*:

$$D=\frac{A(R^2-r^2-c^2)+(r^2-R^2)}{c}, \qquad F=\frac{D^2}{4(A-1)}-r^2 \tag{9}$$

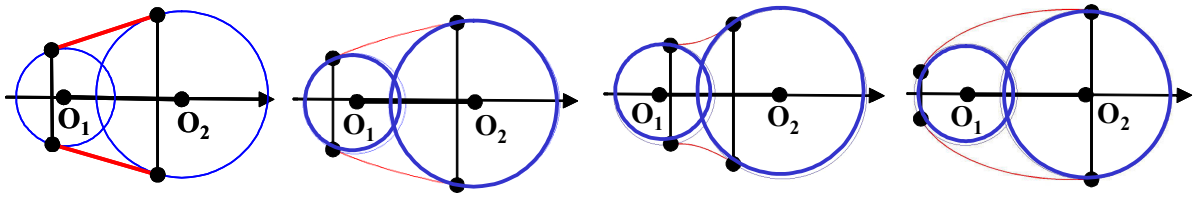

Fig. 3. The RQ-Sphere schemes (a) Cone-sphere (b) Paraboloid-sphere (c) Hyperboloid-Sphere (d) Ellipsoid-Sphere.

4.2 Shape Analysis and the Role of A

As shown in Fig. 3, there are four cases of the shape of RQ: common tangential hyperboloid, ellipsoid, paraboloid and truncated cone, depending on the value of the coefficient *A*. We discuss the impact of *A* on the shape of common tangential revolute quadric.

(1) If $A = 0$, Eq. (6) is reduced to $y^2 + Dx + F = 0$;

(2) If $A \neq 0$, Eq. (6) can be transformed into

$$A\left(x+\frac{D}{2A}\right)^2+y^2=G, \tag{10}$$

where

$$G=\frac{D^2}{4A}-F=\frac{D^2}{4A}-\frac{D^2}{4(A-1)}+r^2=D^2\frac{-1}{4A(A-1)}+r^2 \tag{11}$$

The *x*-coordinates of the tangent points on the two end spheres S_1 and S_2 can be written as:

$$T_{x1}=\frac{-D}{2(A-1)}, \quad T_{x2}=\frac{-(D+2c)}{2(A-1)} \tag{12}$$

Practically, we require that $T_{x1} \le T_{x2}$; thus $T_{x2}-T_{x1}=\frac{c}{1-A}$ implies $A < 1$, since $c > 0$. Furthermore, we can classify the scope of *A* as follows:

(2.1) when $0 < A < 1$, $G > 0$, the corresponding RQ of equation (10) is an ellipsoid;

(2.2) when $G = 0$, the corresponding RQ of equation (10) is a truncated cone. So cone-sphere is just a special case of RQ-Sphere decomposition;

(2.3) when $A < 0$ and $G > 0$, the corresponding RQ of equation (10) is a hyperboloid of one leaf.

(2.4) when $A < 0$ and $G < 0$, the corresponding RQ of equation (10) is a hyperboloid of two leaves.

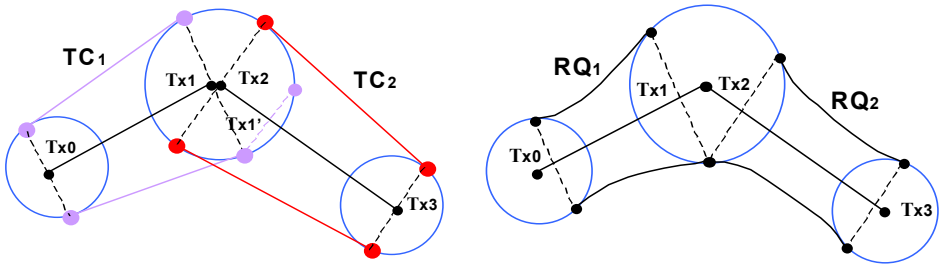

(1) Self-intersection of cone-sphere fitting (2) No self-intersection of RQ-Sphere fitting

Fig. 4. Avoiding self-intersection of RQ-Sphere fitting.

When the shape of canal surface becomes complex in cone-sphere fitting, e.g. when the curvature of the spine curve changes acutely, two adjacent fitting truncated cones TC_1 and TC_2 may intersect each other as shown in Fig. 4, it is noted as self-intersection. For three specified sampling spheres, such self-intersection seems unavoidable in this case.

However, for two fitting revolute quadrics, such self-intersections can be avoided by adjusting the free coefficient *A* of the two fitting *RQ*s flexibly. This leads to two questions: (*i*) how to judge such self-intersection of two fitting *RQ*s and (*ii*) how to adjust the free coefficient A to avoid the self-intersection of two fitting *RQ*s. To the first question, we give a necessary and sufficient condition for the determination. Actually, determining intersections of two fitting *RQ*s in 3D space is equivalent to checking if their generatrices (two planar conic arcs) have intersections in 2D profile space as shown in the following figure; but determining intersection of two conic arcs requires solution of quartic equation in general. Here, we give a much simpler method to determine intersections of two adjacent fitting *RQ*s at their common jointed sphere *O*.

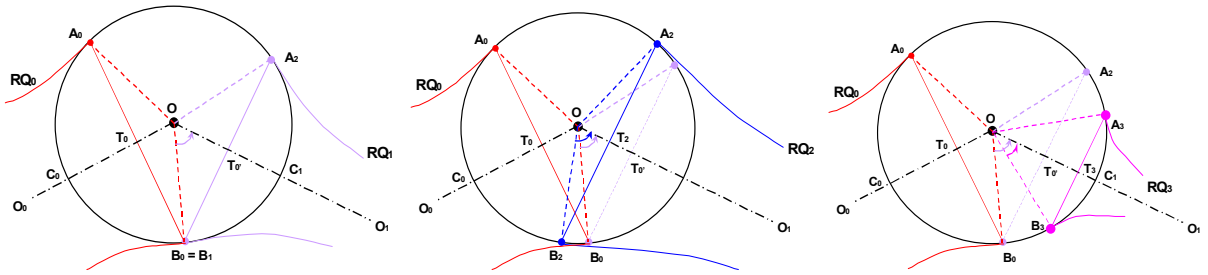

(a) two RQs are tangential (b) two RQs are overlapping (c) two RQs are separated

Fig. 5. Three cases of two adjacent fitting RQs.

By definition, the two RQs are tangent to the common sphere O at the two ending characteristic circles, whose projecting chords is A_0B_0 and one of A_1B_1, A_2B_2 and A_3B_3 as shown in (*a*), (*b*) and (*c*) of Fig. 5 respectively. The RQ_1 and RQ_2 overlap each other if and only if their ending characteristic circles of the common tangent sphere *O* cross each other. This problem is equivalent to the intersection of the two chords A_0B_0 and A_iB_i (*i = 1, 2, 3*) in the circle *O* in 2D projecting space. Assuming T_{x0} is the projection of B_0 onto the revolute axis OO_1, T_i is the projections of chords A_iB_i (*i = 1, 2, 3*) onto the revolute axis OO_1, the necessary and sufficient condition for intersections of two chords A_0B_0 and A_iB_i (*i = 1, 2, 3*) in the circle can be given as follows:

Theorem 2. Two adjacent revolute quadrics RQ_1 and RQ_2 have the common joint sphere, they overlap each other if and only if two corresponding chords A_0B_0 and A_1B_1 intersect each other, furthermore, if and only if $||OT_{0'}|| > ||OT_1||$ holds.

Proof: The two chords A_0B_0 and A_1B_1 intersect each other if and only if two corresponding arcs $\overset{\frown}{A_0C_0B_0}$ and $\overset{\frown}{A_1C_1B_1}$ overlap each other on the same tangent circle O.

1. if $\overset{\frown}{A_0C_0B_0}$ and $\overset{\frown}{A_1C_1B_1}$ overlap, then $\angle B_0OO_0 < \angle B_0OO_1$, then, $r_* sin\angle B_0OO_0 < r_* sin\angle B_1OO_1$, thereby, $||OT_{0'}|| > ||OT_1||$;
2. if $||OT_{0'}|| > ||OT_1||$, then, $||OT_{0'}||/r > ||OT_1||/r$, and conversely, $cos\angle B_0OO_0 < cos\angle B_1OO_1$, then $\angle B_0OO_0 > \angle B_0OO_1$, so there is an overlap between two arcs $\overset{\frown}{A_0C_0B_0}$ and $\overset{\frown}{A_1C_1B_1}$.

We can ensure the avoidance of self-intersection of two adjacent fitting RQ-spheres by adjusting a free parameter *A* to keep $||OT_{0'}|| > ||OT_1||$ during RQ-sphere marching, generally, there are three cases, (*i*) $||OT_{0'}|| > ||OT_1||$; (*ii*) $||OT_{0'}|| > ||OT_1||$ and (*iii*) $||OT_{0'}|| > ||OT_1||$. Geometrically, $||OT_{0'}||$ and $||OT_1||$ are easier to compute than their corresponding chords A_0B_0 and A_1B_1.

4.3 Locally Optimal RQ-Sphere Fitting

By sampling a canal surface $x = x(u,v)$, $y = y(u,v)$ and $z = z(u,v)$ with ($u_i = u_0, u_1, \ldots\ldots, u_m$ and $v_i = v_0, v_1, \ldots\ldots, v_n$, the least square fitting method is employed to determine the best value for *A* in the sense of minimizing the overall sum of square distances of the sampling points (x_{ij}, y_{ij}, z_{ij}) to the fitting RQ-sphere pairs, which can be represented as:

$$\min_{A,D,F} f(A,D,F) = \sum_{i,j} (Ax_{ij}^2 + y_{ij}^2 + z_{ij}^2 + Dx_{ij} + F)^2 \qquad (13)$$

By differentiating (13) with respect to *A*, we get

$$\min f'_A(A,D,F) = 2\sum_{i,j}^{N}(Ax_{ij}^2 + y_{ij}^2 + z_{ij}^2 + Dx_{ij} + F)(x_{ij}^2 + D'_A x_{ij} + F'_A) \tag{14}$$

By substituting the following formulae:

$$D = mA+n,\ D'_A = m\ ,\ F = \frac{(mA+n)^2}{4(A-1)} - r^2\ ,\ F'_A = \frac{2(mA+n)m(A-1)-(mA+n)^2}{4(A-1)^2} = k_0 + \frac{k_2}{4(A-1)^2},$$

where $k_0 = m^2/4$ and $k_2 = (m-n)^2$ into (14), we obtain an optimization equation about A as follows:

$$f'(A) = 2\sum_{i,j}^{N}\left(Ax_{ij}^2 + y_{ij}^2 + z_{ij}^2 + (mA+n)x_{ij} + \frac{(mA+n)^2}{4(A-1)} - r^2\right)\left(x_{ij}^2 + mx_{ij} + k_0 + \frac{k_2}{4(A-1)^2}\right),$$

$$f'(A) = 2\sum_{i,j}^{N}\Big(Ax_{ij}^2(x_{ij}^2 + mx_{ij} + k_0) + (x_{ij}^2 + mx_{ij} + k_0)(y_{ij}^2 + z_{ij}^2 - r^2) + (mA+n)x_{ij}(x_{ij}^2 + mx_{ij} + k_0)$$

$$+ \frac{(x_{ij}^2 + mx_{ij} + k_0)(mA+n)^2}{4(A-1)} + \frac{Ax_{ij}^2 k_2}{4(A-1)^2} + \frac{(y_{ij}^2 + z_{ij}^2 - r^2)k_2}{4(A-1)^2} + \frac{(mA+n)x_{ij}k_2}{4(A-1)^2} + \frac{(mA+n)^2 k_2}{16(A-1)^3}\Big) = 0,$$

$$M_0 A(A-1)^3 + M_1(A-1)^3 + M_2(mA+n)(A-1)^3 + M_0(mA+n)^2(A-1)$$

$$+ M_3 k_2 A(A-1) + M_4 k_2 A(A-1) + M_5(mA+n)k_2 + (mA+n)^2 k_2 = 0 \tag{15}$$

where

$$M_0 = \frac{16}{N}\sum_{i,j}^{N} x_{ij}^2(x_{ij}^2 + mx_{ij} + k_0),\quad M_1 = \frac{16}{N}\sum_{i,j}^{N}(y_{ij}^2 + z_{ij}^2 - r^2)(x_{ij}^2 + mx_{ij} + k_0),$$

$$M_2 = \frac{16}{N}\sum_{i,j}^{N} x_{ij}(x_{ij}^2 + mx_{ij} + k_0),\quad M_3 = \frac{4}{N}\sum_{i,j}^{N} x_{ij}^2,\quad M_4 = \frac{4}{N}\sum_{i,j}^{N}(x_{ij}^2 + mx_{ij} + k_0),\quad M_5 = \frac{4}{N}\sum_{i,j}^{N} x_{ij}$$

Equation (15) is a quartic with closed form solutions to A, D and F for a locally optimal RQ-sphere fitting canal surfaces.

4.4 Global RQ-Sphere Fitting

The fitting method presented in the previous subsection provides a locally optimal GC^1 RQ-sphere approximation to canal surfaces for two arbitrary sampling points onto the spine curve. Naturally, the next concern is to globally fit the canal surface by a sequence of RQ-sphere pairs within a specified error tolerance e. We introduce an adaptive error-driven bi-section marching method that uses RQ-sphere fitting method as a basic procedure. The error metric used this time is the Hausdorff distance between the canal surface and the fitting RQ-sphere. The algorithm is detailed below:

Algorithm 1. Global_RQ_Sphere_Fitting(e, t_s, t_e)

//* fitting the canal surface between t = t_s and t = t_e at the tolerance e *//

(1) $t_1 \leftarrow t_s$, $t_2 \leftarrow t_e$;
(2) fit the canal surface between $[t_1, t_2]$ with a RQ-sphere with the optimal RQ-sphere fitting in 4.3;
(3) calculate the error d between the canal surface and the fitting RQ-sphere;
(4) if $d > e$, shorten the fitting interval, $t_2 \leftarrow (t_1 + t_2)/2$, goto (2); // to fit it again on the new $[t_1, t_2]$
(5) if ($d < e$) and ($t_2 < t_e$), extend the fitting interval by setting $t_2 \leftarrow (t_e + t_2)/2$, and goto (2);
(6) output the fitting interval $[t_1, t_2]$ and its corresponding RQ-sphere;
(7) if $t_2 == t_e$, goto (9);
(8) else $t_1 \leftarrow t_2$; $t_2 \leftarrow t_e$; goto (2) for the next RQ-sphere;
(9) return.

---

5. COMPUTING PLANAR SECTIONS OF A CANAL SURFACE

In this section, we apply RQ-sphere decomposition to computing planar sections of canal surfaces. RQ-sphere decomposition reduces computing plane/canal intersection to computing plane/RQ intersection, which could be solved

robustly, efficiently and accurately with the geometric methods in [25] and [26]. For efficient intersection determination, valid intersection intervals (VII) and bounding cylinder clipping (BC clipping) are proposed in the two subsequent subsections 5.1 and 5.2 respectively and two implemental examples in 5.3 show effectiveness of our proposed algorithm.

5.1 Binary Bounding Cylinder Tree (BCT) and Valid Intersection Intervals (VII)

Although a canal surface is approximated as *n* RQ-spheres, sometimes, usually, only few of them overlap with the plane, it is really unnecessary to take intersection test for all RQs with the plane. Therefore, it is quite necessary to cull those overlapping RQ-spheres with the cutting plane before the formal intersection computing. For that purpose, we organize binary bounding cylinder tree BCT hierarchically and cull those overlapping RQs by BC-clipping for the cutting plane. We choose bounding cylinder to enclose canal surfaces or RQs because (*i*) it can enclose them more tightly than traditional bounding box and bounding sphere, (*ii*) determine valid intersection intervals of plane and BC. BCT is constructed in the bottom-up bisection way shown in Fig. 6(a).

(1) To construct a bounding cylinder BC_i for each RQ_i of the subdivided canal surface (i = 0,1,2,…n) as the bottom level of BCT;

(2) To construct a big BC for each pair of neighboring bounding cylinders BC_{2m} and BC_{2m+1} (m = 0,1,2,…n/2) as the second level of BCT, for example, two given bounding cylinders BC_0 and BC_1, and a big bounding cylinder BC_4 is constructed geometrically, in this bottom-up manner, a binary bounding cylinder tree BCT can be organized hierarchically and recursively.

To cull those overlapping RQ which are valid for intersection computing from all subdivided RQs, we defined a new concept, Valid Intersection Intervals (VII), as *t*-intervals corresponding to the overlapped parts of a plane and a canal surface in Fig. 6(b). Furthermore, a new idea of *bounding cylinders clipping*, hereafter denoted by *BC clipping*, is devised to detect all the potential RQ candidates, that will be illustrated in the next subsection.

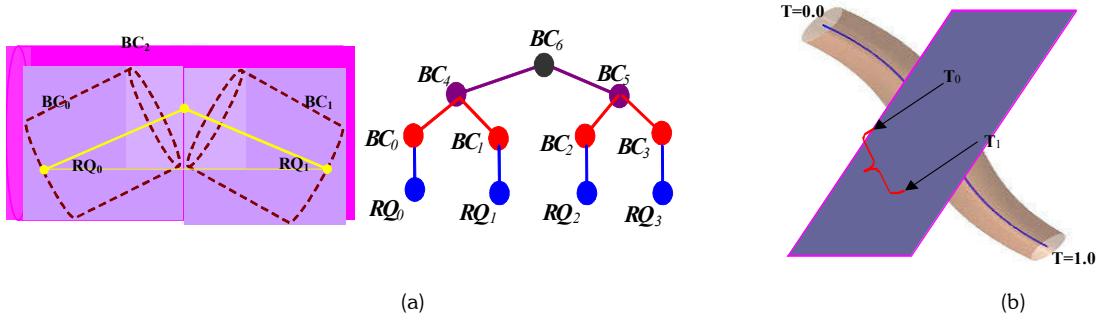

Fig. 6. (a) Binary bounding cylinder tree; (b) The valid intersection intervals VII for plane/canal intersection.

5.2 Plane Clipping Bounding Cylinder

Normally, VII can be found by taking a binary search in BCT with $O(log N)$, where N is the total number of RQs. However, the efficiency can be further accelerated by our proposed BC clipping.

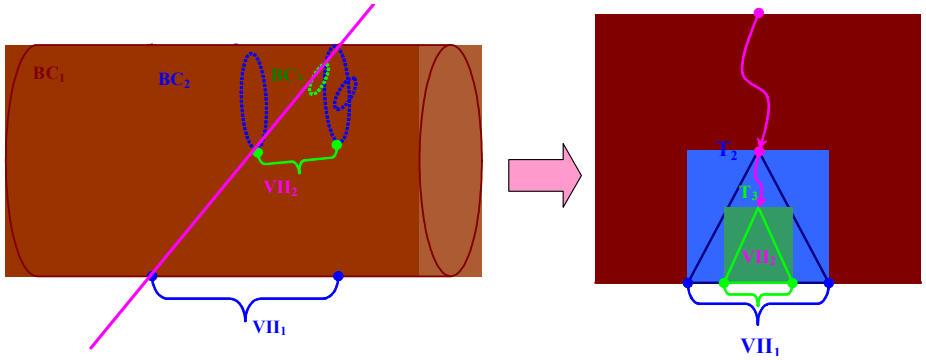

Fig. 7. Clipping BC by plane and reducing the depth of searching for BCT with 2 consecutive rounds.

As shown in Fig. 7, the first round of plane-clipping-BC, the intersection interval of $\mathbf{BC_1}$ is reduced to an initial (blue) intersection interval $\mathbf{VII_1}$. Correspondingly in **BCT**, the tree $\mathbf{T_1}$ is reduced to a smaller one $\mathbf{T_2}$, then, all corresponding RQs within $\mathbf{VII_1}$ form a new bounding cylinder $\mathbf{BC_2}$, which is smaller than $\mathbf{BC_1}$.
After the second round of plane-clipping-BC, the intersection interval $\mathbf{VII_1}$ is further reduced to a smaller one $\mathbf{VII_2}$. Correspondingly in **BCT**, $\mathbf{T_2}$ is reduced to a further smaller subtree $\mathbf{T_3}$. In the same manner, the current intersection interval can be refined recursively, which correspond to all the valid *RQ*s at the specified tolerance.
This intersection determination of VII is a hybrid method, which interleaves *range searching* and binary search according to the 70% clipping criterion: if the size of intersection interval $\mathbf{T}_{i+1}$ can be reduced out by more than 30% of $\mathbf{T}_i$ through *BC clipping*, we adopt *range search*; otherwise, switch to the normal binary search. *BC clipping* requires computing the intersection interval of plane and cylinder frequently, which can be done by solving only linear equations. Of course, the extent of each round shrinking VII depends on canal shape, relative positions and orientations between the plane and canal surface. We still use binary search when plane and canal are not in a good configuration with respect to each other.

5.3 Tracing Intersection Curves

After BC clipping, we get a set of valid t-intervals, $[t_0, t_1]$, $[t_1, t_2]$, … $[t_i, t_{i+1}]$, …, $[t_{n-1}, t_n]$ $(0.0 \le t_0 \le t_1 \le 1.0)$, for all the RQ-spheres of each $[t_i, t_{i+1}]$, their planar sections, conic arcs (intersection curves of plane/RQ) or circular arcs (plane/sphere) RQ-sphere can be computed by using geometric methods [25] and [26]. Therefore, planar sections of a canal surface could be represented as a series of G^1 conic segments that can be easily organized as closed loops, open branches and isolated points, by tracing these conic arcs (plane/RQ intersection curves) segment by segment sequentially and checking the types of these valid intersection intervals:

- *Isolated point*. There are two cases for producing isolated points:
  - When $[t_i, t_{i+1}]$ degenerates into a single point, that means $t_i, = t_{i+1}$, geometrically, the plane becomes tangential to one RQ or spherical stripe;
  - When the plane just touches the beginning or ending characteristic circle of the canal surface, in both cases, the singularity occur.
- *Closed loops*. For those inner t-intervals $[t_i, t_{i+1}]$ where i = 1, 2, … n-2, they produce a closed loops onto the final intersection intervals correspondingly. Of course, some of them might be in the eight-cross shape when the plane touches tangentially some characteristic circles of canal surface.
- *Open branch*. For the first and last interval $[t_0, t_1]$ and $[t_{n-1}, t_n]$, we need to check if either the beginning characteristic circle is (1) cut or (2) touched tangentially by the plane, in the case (1), either the first branch or last branch is an open branch; in the case (2), but the plane just tangentially contacts the two bounding circles of canal surface, this branch still is closed loop.

6. EXAMPLES

We implemented two examples of RQ-sphere decomposition and planar sections respectively for canal surfaces with *VC++* and *OpenGL*, under Windows *XP* on a PC (Pentium III, 512MB RAM), Both the spine curve and radius function of canal surfaces are represented by cubic Beizer form in given examples.

(a) a helix canal surface (b) a tree with 13 canal surfaces

Fig. 8. RQ decompositions of two objects made up of one or more canal surfaces.

6.1 Examples of RQ-sphere Decomposition

Two examples of RQ-sphere decomposition are presented in Fig. 8. The first example is a canal surface with a helix curve as its spine. The second is a tree-like shape composed from 13 canal surfaces. For the purpose of comparison, cone-sphere decomposition was also programmed, and some comparative results are given in the following Table 1, it show that RQ-sphere performs more efficiently and smoothly than cone-sphere for same canal surfaces

Tolerance	*No. of cone-sphere pairs*	*No. of RQ-sphere pairs*
Example 1 at $5x10^{-4}$	235	175
Example 2 at $5x10^{-3}$	2123	768
Example 3 at $5x10^{-4}$	1373	636

Table 1. Comparison of cone-sphere vs. RQ-sphere decompositions on example.

6.2 Examples of Planar Section Computing

Two examples have been developed based on RQ-sphere decomposition and BC clipping. A single-branch and a double-branch planar section curves of canal surfaces are shown in Fig. 9(a) and Fig. 9(b) respectively. Both examples can be generated in a few *milliseconds*. The implemented results verify the effectiveness of our proposed method.

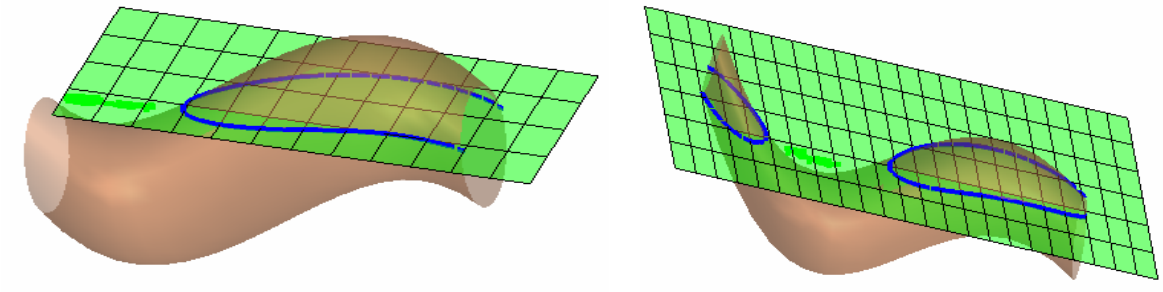

(a) (b)

Fig. 9. Plane intersecting a canal surface, with (a) single-branch curve and (b) double-branch curves.

6. CONCLUSIONS

In this paper, firstly, we briefly present a methodology to check for regularity of a canal surface. Then, a new method for approximation of canal surfaces with RQ-spheres was presented. This approximation improves upon traditional cone-spheres in two ways: at same tolerance, significantly fewer RQ-spheres approximate a given canal surface; secondly, self-intersection can be avoided due to the added flexibility in local approximation. The RQ-sphere decomposition was used to develop efficient intersection algorithms involving canal surfaces, and examples of planar intersection were presented.

Canal surfaces occur very often in CAD and graphics, and therefore it is interesting to study specialized approximations for them. There are various applications of such approximations in CAD, especially intersections and surface reconstruction from skeletal data. The RQ-sphere is shown to be superior to the commonly used cone-sphere, since the latter (1) fails to provide an approximation at high tolerances, and (2) uses significantly larger number of atomic pairs than the former at any given tolerance level. But it still requires dense RQ-spheres to approximate canal surfaces where the spine curve bends at high curvature. Thus, more efficient and stable quadric decomposition for canal surfaces is an appealing task and how to apply the proposed quadric decomposition to other geometric problems of canal surfaces is also our future work. Further, it may be possible to use our local RQ-sphere fitting to detect potential locations of singularity in a canal surface, an application that we are now investigating.

7. ACKNOWLEDGEMENTS

The authors thank the support of Departments of Computer science, Industrial Engineering and Logistics Management, and Mechanical Engineering. The research was partially supported by a RGC CERG grant (Grant No. HKUST6235/02

8. REFERENCES

[1] Bangert, C. and Prautzsch, H., Quadric spline, *CAGD*, Vol. 16, No. 6, 1999, pp 497-515.

[2] Bangert, C. and Prautzsch, H., A geometric criterion for the convexity of Powell-Sabin interpolants and its multivariate generalization, *CAGD*, Vol. 16, No. 6, 1999, pp 529-538.
[3] Dahmen, W., Smooth piecewise quadric surfaces, *Mathematical methods in computer aided geometric design*, Lyche, T. and Schumaker, L. (Eds.), Academic Press, 1989, pp 181-194.
[4] Ferly, E., Gascuel, C. M-P, Attali, D., Skeletal reconstruction of branching shapes, *Implicit Surfaces'96*, (The Second International Workshop on Implicit Surfaces), pp. 127-142, Eindhoven, Netherlands, October, 1996.
[5] Froumentin, M. and Chaillou, C. Quadric surfaces: a survey with new results, *Mathematics of Surfaces VII*, pp. 363-381, Tim Goodman and Ralph Martin (Eds.), 1997.
[6] Günter, A., Canal surfaces versus normal ringed surfaces, *CAGD*, Vol. 11, No. 4, 1994, pp 475-476.
[7] Landsmann, G., Schicho, J., Winkler, F. and Hillgarter, E., Symbolic parameterization of pipe and canal surfaces, *Proceedings of ISSAC* '00, St. Andrews, Scotland, 2000.
[8] Gelston, S. M. and Dutta, D., Boundary surface recovery from skeleton curves and surfaces, *CAGD*, Vol. 12, No. 2, 1995, pp 27-51.
[9] Guo, B., Quadric and cubic bitetrahedral patches, *The Visual Computer*, Vol. 7, No. 5, 1995, pp 253-262.
[10] Guo, B., Representation of arbitrary shapes using implicit quadrics, *The Visual Computer*, Vol. 9, No. 5, 1993, pp 267-277.
[11] Heo, H. S., Hong, S. J., Seong, J. K. and Kim, M. S., The intersection of two ringed surfaces and some related problems, *Graphical Model*, Vol. 63, No. 4, 2001, pp 228-244.
[12] Johnstone J., A new intersection algorithm for cyclides and swept surfaces using circle decomposition, *CAGD*, Vol. 10, No. 1, 1993, pp 1-24.
[13] Kim, K.-J. and Lee, I.-K., The Perspective Silhouette of a Canal Surface, *Computer Graphics Forum*, Vol. 22, No. 1, 2003, pp 15-22, March.
[14] Kim, K.-J. and Lee, I.-K., Computing Isophotes of Surface of Revolution and Canal Surface, *CAD*, Vol. 35, No. 3, 2003, pp 215-223.
[15] Kim, K. J., Minimum distance between a canal surface and a simple surface. *CAD*, Vol. 35, No. 10, 2003, pp 871-879.
[16] Lee, I. K., Reconstruction of Pipe and Canal Surfaces Using Shrinking Method, *Technical Report, PIRL-TR-99-001*, POSTECH Information Research Laboratories, August, 1999.
[17] Max, N., Cone-spheres, *ACM SIGGRAPH Computer Graphics*, Vol. 24, No. 4, 1990, pp 59-62.
[18] Nishita, T. and Hohan, H., A scan line algorithm for rendering curved tubular objects, *Proceedings of Pacific Graphics*, 1999, pp 92-101.
[19] Paluszny, M. and Bühler, K., Canal Surfaces and Inversive Geometry, *Mathematical Methods for Curves and Surfaces II*, Daehlen M., Lyche T. and Schumaker L.L. (Eds.), 1998, pp 367-375.
[20] Peternell, M. and Pottmann, H., Computing rational parameterizations of canal surfaces, *Journal of Symbolic Computation*, Vol. 23, No. 2, 1997, pp 255-266.
[21] Powell, M. J. D. and Sabin, M. A., Piecewise quadratic approximations on triangles, *ACM Transaction on Mathematical Software*, Vol. 3, 1997, pp 316-325.
[22] Maekawa, T. and Patrikalakis, N. M., Sakkalis, T. and Yu, G., Analysis and applications of pipe surfaces, *CAGD*, Vol. 15, No. 5, 1998, pp 437-458.
[23] Sederberg, T., Piecewise algebraic surface patches, *CAGD*, Vol. 2,No. 1, 1985, pp 53-60.
[24] Willemans, K. and Dierckx, P., Surface fitting using convex Powell-Sabin splines, *Journal of Computational and Applied Mathematics*, Vol. 56, No. 3, 1994, pp 263-282.
[25] Miller, J. R. and Goldman, R. N., Using tangent ball to find plane sections of natural quadrics, *IEEE Computer Graphics & Applications*, Vol. 12, No. 2, 1992, pp 68-82.
[26] Shene, C. and Johnstone, J. K., Computing the intersection of a plane and a revolute quadric, *Computer & Graphics*, Vol. 18, No. 1, 1994, pp 47-60.